A continuous parameterization of the cosmic web

C.Yamila Yaryura^{1,2,*} Mario G. Abadi^{1,2}, Noam I. Libeskind³, Stefan Gottlöber³, Sofía A. Cora^{4,5} and Gustavo Yepes^{6,7}

- CONICET-Universidad Nacional de Córdoba, Instituto de Astronomía Teórica y Experimental (IATE), Laprida 854, X5000BGR, Córdoba, Argentina
- Observatorio Astronómico, Universidad Nacional de Córdoba, Laprida 854, X5000BGR, Córdoba, Argentina
- Leibniz-Institut für Astrophysik Potsdam (AIP), An der Sternwarte 16, D 14482, Potsdam, Germany
- Instituto de Astrofísica de La Plata (CCT La Plata, CONICET,UNLP), Observatorio Astronómico, Paseo del Bosque,
- Facultad de Ciencias Astronómicas y Geofísicas, Universidad Nacional de La Plata (UNLP), Observatorio Astronómico,
- Departamento de Física Teórica M-8, Universidad Autónoma de Madrid, Cantoblanco, E-28049 Madrid, Spain
- Centro de Investigación Avanzada en Física Fundamental (CIAFF), Universidad Autónoma de Madrid, E-28049 Madrid, Spain

ABSTRACT

The intrinsic properties of galaxies are influenced by their environments, underscoring the environment's critical role in galaxy formation and evolution. Traditionally, these environments are categorized into four fixed classifications: knots, filaments, walls, and voids, which collectively describe the complex organization of galaxies within large-scale structures. We propose an alternative description that complements the traditional quadripartite categorization by introducing a continuous framework, allowing for a more nuanced examination of the relationship between the intrinsic properties of galaxies and their environments. This complementary description is applied using one of the most prevalent methodologies: categorization using the eigenvalues of the Hessian matrix extracted from the matter density field. We integrated our findings into a semi-analytical model of galaxy formation, combined with cosmological numerical simulations, to analyze how the intrinsic properties of galaxies are influenced by environmental changes. In our study, we find a continuous distribution of eigenvalue ratios, revealing a clear dependence of galaxy properties on their surrounding environments. This method allowed us to identify critical values at which transitions in the behavior of key astrophysical galaxy

Key words. Cosmology: large-scale structure of Universe – Galaxies: kinematics and dynamics

Córdoba, Argentina

2 Observatorio Astronómico, Universidad Nacional de Córdoba, I
3 Leibniz-Institut für Astrophysik Potsdam (AIP), An der Sternwe
4 Instituto de Astrofísica de La Plata (CCT La Plata, CONICET,U
1900FWA, La Plata, Argentina
5 Facultad de Ciencias Astronómicas y Geofísicas, Universidad N
Paseo del Bosque, B1900FWA La Plata, Argentina
6 Departamento de Física Teórica M-8, Universidad Autónoma de
7 Centro de Investigación Avanzada en Física Fundamental (CIAI

ABST

The intrinsic properties of galaxies are influenced by their envir formation and evolution. Traditionally, these environments are c and voids, which collectively describe the complex organization o description that complements the traditional quadripartite categoriz nuanced examination of the relationship between the intrinsic properties of the most prevalent methodole extracted from the matter density field. We integrated our findings cosmological numerical simulations, to analyze how the intrinsic pour study, we find a continuous distribution of eigenvalue ratios, revenvironments. This method allowed us to identify critical values properties become evident.

Key words. Cosmology: large-scale structure of Universe – Gala

1. Introduction

Large galaxy surveys developed in recent years, such as the two degree Field Galaxy Redshift Survey (2dFGRS, Colless et al. 2003) and the Sloan Digital Sky Survey (SDSS; Tegmark et al. 2004), as well as large numerical simulations, show evidence that the distribution of matter in the Universe is a nonrandom distribution. The distribution of matter on megaparsec scales, traced by galaxies, intergalactic gas and dark matter (DM), defines an intricate multiscale interconnected network known as the cosmic web, which characterizes the large-scale structure of the Universe, forms through gravitational instability arising from the initial perturbations in an otherwise homogeneous density field. Two prominent features of this web are immediately apparent. First, it consists of both high-density and density field. Two prominent features of this web are immediately apparent. First, it consists of both high-density and low-density regions. Second, the structures within this network are notably nonspherical, indicating that gravitational collapse is far from isotropic. Thus, the cosmic web emerges from a highly anisotropic gravitational collapse, producing structures that deviate significantly from spherical symmetry. In other words, the morphology of these structures reflects the nature of gravitational collapse, which remains ongoing, since many of these formations have not yet reached virial equilibrium. The low-density regions exist as a consequence of the emergence of

high-density structures, and vice versa. This interdependence implies that the collapse of one structure influences the evolution of others. Hence, the structures within the cosmic web are not isolated, but rather interconnected, dynamically shaping each

While the cosmic web exhibits a continuous and interconnected structure, describing it through distinct classifications offers a commonly used framework for analyzing the diverse environments in which galaxies reside. The cosmic web is typically categorized into four components: knots (or clusters), filaments, walls (or sheets), and voids. This classification is generally based on the rate of compression or expansion of cosmic material along three orthogonal axes (Icke & van de Weygaert 1991; Cautun et al. 2014; Wang & Kang 2017, among others). Various methods have been developed to perform this classification, each relying on different physical fields (such as density or velocity) and employing different techniques. Over the past few decades, these methods have proliferated and can broadly be grouped into five categories (Forero-Romero et al. 2025): (i) Hessian-based methods (geometric and multi-scale; e.g., Forero-Romero et al. 2009; Hoffman et al. 2012); (ii) graph-based methods (e.g., Alpaslan et al. 2014); (iii) stochastic methods (e.g., Tempel & Tamm 2015); (iv) topological methods (e.g., Sousbie 2011; Aragón-Calvo et al. 2010); and (v) phase space methods (e.g., Falck et al. 2012). These approaches rely

^{*} yamila.yaryura@unc.edu.ar

on the definition of specific threshold values to categorize different environments. As a result, the classifications obtained naturally reflect the methodological design and parameter choices of each technique. While this does not undermine their usefulness, it highlights the importance of carefully considering how such definitions may influence the interpretation of galaxy–environment relations.

The theoretical foundation for applying tidal and deformation tensors in the study of the cosmic web was laid by early works such as Shandarin & Zeldovich (1989), which demonstrated how anisotropic structures naturally arise from gravitational instability. Subsequent studies (e.g., Shandarin 2004; Shandarin et al. 2012) further emphasized the role of multi-stream flows and the geometry of the deformation tensor in shaping filaments and sheets, thereby providing the conceptual basis for many of the classification schemes currently in use. These developments strongly motivated the adoption of Hessian-based approaches (Olex et al. 2025), where the eigenvalues of the Hessian matrix capture the local dynamical behavior of matter and serve as key indicators for identifying different environments within the cosmic web.

The commonly used Hessian-based methods are based on the Hessian matrix generated from a continuous field. This matrix is diagonalized to estimate its eigenvalues and eigenvectors. In this method, a threshold is commonly applied to the eigenvalues of the Hessian matrix, typically set to zero ($\lambda_{th} = 0$). When the field used is the density field, the sign of a given eigenvalue at a given point determines whether the gravitational force in the direction of the corresponding eigenvector is contracting (a positive eigenvalue) or expanding (negative). So, the classification of the cosmic web into four distinct categories is performed according to the number of eigenvalues exceeding the established threshold. Numerous studies have analyzed the most appropriate value for this threshold according to the problem that is being addressed address (Hahn et al. 2007b; Forero-Romero et al. 2009; Libeskind et al. 2012, 2013, 2014). Consequently, alongside the intrinsic characteristics of the method, the resulting classification is naturally shaped by the specific threshold value adopted for the analysis.

One of the primary aims in developing methods for classifying the cosmic web is to determine whether, and how, the cosmic web influences the properties of galaxies and their evolution within it. There is clear evidence that the properties of DM halos and galaxies (such as shape, spin, color, star formation rate, and the spatial distribution of satellites) are correlated with their large-scale environments (Aragón-Calvo et al. 2007; Hahn et al. 2007b,a; Zhang et al. 2009; Hahn et al. 2010; Codis et al. 2012; Aragon-Calvo & Yang 2014; Codis et al. 2015; Zhang et al. 2015, among others). To understand how the large-scale structure and the immediate environment of a halo or galaxy affect its formation and evolution, it may be very useful to use a continuous description of the cosmic web. The traditional discrete classification has undoubtedly proven to be a valuable tool, with successful applications across different fields, from botany to cosmology, as it provides a practical framework for initiating scientific discussions and formulating qualitative insights. A continuous parameterization does not replace this approach, but rather complements it by enabling a more refined and detailed study of the dependence of galaxy properties on the surrounding environment.

In this paper we present a simpler and continuous description of the cosmic web. We computed the Hessian matrix from the density field, which was derived from the matter distribution traced by the positions of DM particles in a cosmological simulation. We propose describing the cosmic web continuously, without categorizing it into separate classes, through direct comparisons of the rates of compression (or expansion). This information was derived from the analysis of a DM-only simulation, and we established the connection to galaxy properties by integrating the simulation with a semi-analytic model of galaxy formation. This paper is organized as follows. We describe the DM-only simulation and the semi-analytic model used in Section 2. In Section 3, we describe the method applied to classify the cosmic web based on eigenvalues estimated from the diagonalized Hessian matrix generated from the spatial distribution of the DM particles. In Section 4, we analyze the dependence of both the galaxy stellar mass and its DM halo mass on the surrounding environment. In Section 5, we examine the influence of a galaxy's environment on its main dynamical properties, utilizing the cosmic web description presented in this work. Finally, in Section 6, we highlight the key findings of our study.

2. Hybrid model of galaxy formation

The galaxy sample is extracted from a catalog generated using a hybrid model that combines a semi-analytical approach to galaxy formation and evolution with a DM-only cosmological simulation. Below, we briefly describe the main aspects of this model.

2.1. Dark matter cosmological simulation

We used the smdpl DM-only cosmological simulation , which follows the evolution of 3840^3 particles from redshift z=120 to z=0, within a (relatively) small volume (a periodic box of sidelength of $400\,\mathrm{Mpc}\,h^{-1}$). This large number of particles within such a volume reaches a mass resolution of $9.63\times10^7\,\mathrm{M}_\odot\,h^{-1}$ per DM particle (see Klypin et al. 2016 for more details). SMDPL cosmological parameters are given by a flat Λ cold DM model consistent with Planck measurements: $\Omega_\mathrm{m}=0.307$, $\Omega_\mathrm{B}=0.048$, $\Omega_\Lambda=0.693$, $\sigma_8=0.829$, $n_\mathrm{s}=0.96$, and h=0.678 (Planck Collaboration et al. 2014).

The Rockstar halo finder (Behroozi et al. 2013a) is used to identify DM halos keeping just overdensities with at least $N_{\min} = 20$ DM particles. There are two classifications of DM halos: main host halos (detected over the background density) and subhalos (that lie inside other DM halos). From these halos, ConsistentTrees (Behroozi et al. 2013b) constructs merger trees, by linking halos and subhalos forward and backward in time to progenitors and descendants, respectively.

2.2. Semi-analytic model of galaxy formation, sag

We used the latest version of the semi-analytic model sag described in Cora et al. (2018), which is based on the model presented by Springel et al. (2001). This is an updated and

¹ https://www.cosmosim.org/metadata/smdpl/

improved version, including the main physical processes required for galaxy formation; we refer the reader to Cora et al. (2018) for a detailed and exhaustive description of the model. Each sag galaxy populates a DM halo of the simulation in such a way that central galaxies correspond to main host halos while satellite galaxies are hosted by subhalos, according to the information provided by the merger trees. These satellites are defined as orphans when the mass of their DM substructures is no longer detected by the halo finder. However, in this work we focused only on central galaxies. To regulate the physical processes involved in the sag model, a set of free parameters are employed. These parameters are calibrated using a set of observed galaxy properties. The particle swarm optimization technique (Kennedy & Eberhart 1995) and the observational data presented in Knebe et al. (2018) were used to select the best-fitting values for the free parameters of sag for the SMDPL simulation (Ruiz et al. 2015). The reader can refer to Table 1 in Yaryura et al. (2023), where these best-fitting values are listed.

3. Tidal field estimation

In recent decades, numerous methods have been developed to classify the cosmic web (see Libeskind et al. 2018, for a review). Many of these methods determine the Hessian matrix from the density, velocity, or potential field using a fixed finite grid. This matrix is diagonalized to determine its eigenvectors and eigenvalues, which provide information about the principal directions of local collapse or expansion. In practice, when estimating the Hessian matrix from the density, what is done is constructing a discrete density field from the discrete distribution of particles using the cloud-in-cell technique with a given number of grids, $N_{\rm grid}^3$. A spherically symmetric Gaussian window function is applied to smooth this density field, obtaining a smoothed, continuous density field, $\rho(x)$. The gravitational potential originated by this distribution obeys the (rescaled) Poisson equation:

$$\nabla^2 \phi = \delta,\tag{1}$$

where ϕ is the gravitational potential rescaled by $4\pi G\bar{\rho}$, $\bar{\rho}$ is the mean cosmological density, and the density contrast (δ) is given by $\delta = \rho/\bar{\rho} - 1$.

Furthermore, the Hessian of the gravitational potential ϕ is sometimes called the deformation tensor (see for example Forero-Romero et al. 2009) and is given by

$$T_{\alpha\beta} = \frac{\partial^2 \phi}{\partial r_\alpha \partial r_\beta},\tag{2}$$

where α and β represent the spatial coordinates x, y and z. By diagonalizing this matrix, its eigenvalues a > b > c are estimated, and they satisfy the following relationship:

$$\delta = a + b + c. \tag{3}$$

These eigenvalues represent the directional changes in the gravitational field's intensity, offering insights into regions of compression or expansion. Specifically, the sign of each eigenvalue at a given point reveals the nature of the gravitational

influence along the direction of its associated eigenvector: a positive value indicates contraction, while a negative value indicates expansion. Starting from the case where all three eigenvalues are positive, to the case where all three are negative, and passing through the intermediate cases, the density decreases.

From these eigenvalues, the cosmic web is commonly classified into four distinct categories: knots, filaments, walls and voids, according to the number of eigenvalues greater than a certain threshold value (λ_{th}):

- Knot: if $\lambda_{\text{th}} < c$ - Filament: if $c < \lambda_{\text{th}} < b$ - Wall: if $b < \lambda_{\text{th}} < a$ - Void: if $a < \lambda_{\text{th}}$

So, this usual cosmic web classification mainly depends on two parameters: the smoothing scale and the threshold value λ_{th} selected. Although $\lambda_{th}=0$ is the most commonly used value (Hahn et al. 2007b), there are numerous studies about the most suitable value for this threshold value (Forero-Romero et al. 2009; Libeskind et al. 2012, 2013, 2014). Several of these works recommend different values depending on the specific research focus (Forero-Romero et al. 2009). For example, in our study of associations of dwarf galaxies within the same simulation, we applied this classification using $\lambda_{th}=0$ (Yaryura et al. 2023). Consequently, this classification is highly sensitive to the selected threshold value.

The complex and continuous nature of the large-scale structure of the Universe motivates the development of alternative methods for characterizing the cosmic web. In this context, we propose a simple and continuous description based on directly examining the ratios of the eigenvalues of the Hessian matrix derived from the matter distribution. We estimated the eigenvalues from the tidal field (e.g., Hahn et al. 2007b) of the DM particle distribution of the parent simulation smppl using the method presented in Libeskind et al. (2013). Based on the position of the DM particles in the smppl simulation, we used a grid of 400^3 cells and three different specific smoothing lengths l=1, 2 or 4 Mpc h^{-1} to estimate the three eigenvalues for each cell. So, to each cell corresponds: a>b>c.

The importance of describing the cosmic web lies, among other factors, in studying where galaxies are preferentially located and how their main properties are influenced by the surrounding environment. The sample of galaxies studied in this work is obtained from a set of semi-analytical galaxies built by enforcing a minimum stellar and halo mass of $M_{\star} = 10^9 \,\mathrm{M}_{\odot} \,h^{-1}$, and $M_{200} = 10^{11} \,\mathrm{M}_\odot \,h^{-1}$ (equivalent to ~ 1000 DM particles), respectively. The final sample has a total of 1688127 well resolved, semi-analytical central galaxies, with stellar masses in the range $9.0 < \log_{10}(M_{\star}[\mathrm{M}_{\odot}\,h^{-1}]) < 12.9$, hosted by DM halos with masses ranging between hosted by DM halos with masses ranging between $11.0 < \log_{10}(M_{200}[M_{\odot}h^{-1}]) < 15.2$. The existence of central galaxies with stellar masses exceeding $10^{12} M_{\odot} h^{-1}$ stems from the current version of sag's inability to accurately fit the massive end of the stellar mass function at z = 0. This leads to an excess of galaxies with stellar mass $M_{\star} \gtrsim 1.3 \times 10^{11} \, M_{\odot} \, h^{-1}$, as already indicated in Cora et al. (2018), where possible causes are proposed.

So, the environment of each simulated galaxy extracted from the sag model is parameterized by the eigenvalues of the cell in

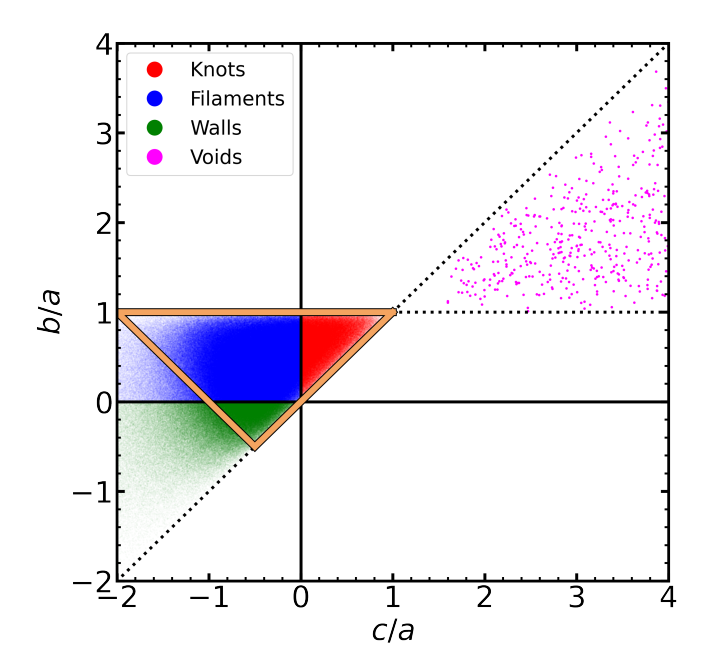


Fig. 1: Relationship between the eigenvalue ratios b/a and c/a for central galaxies, according to conventional classification of the cosmic web, using the threshold $\lambda_{\rm th}=0$. Each point corresponds to one galaxy, which is color-coded according to the eigenvalues associated with the cell it occupies as indicated by the legend. The size of the magenta points has been arbitrarily increased for visibility, as they are very sparse. The dotted black lines delineate the regions that the eigenvalue ratios may occupy. The horizontal dotted black line at b/a=1 indicates that b/a<1 whenever a>0 and b/a>1 only when a<0. The positively sloped dotted black line indicates the condition a>b>c, which implies b/a>c/a if a>0 and b/a<c/a if a<0. The area inside (outside) the orange triangle corresponds to $\delta>0$ ($\delta<0$).

which it is located. To estimate these eigenvalues, we applied a spherically symmetric Gaussian window function to smooth the density field, resulting in a continuous smoothed density field $\rho(x)$. This procedure was performed using different smoothing lengths. We verified that the results obtained in this work do not change significantly when we use different smoothing lengths $(l=1, 2, \text{ or } 4 \text{ Mpc } h^{-1})$. Therefore, for simplicity and clarity, the results of this paper will be presented only for the smoothing length $l=1 \text{ Mpc } h^{-1}$, which is a sufficient volume to analyze the environment of galaxies. In the Appendix A, we present the differences arising from the use of three distinct smoothing scales $(l=1, 2, \text{ or } 4 \text{ Mpc } h^{-1})$, as well as the differences in estimating eigenvalues derived from either the DM density field or the shear velocity field.

Considering the previously described sample of galaxies, we analyzed the properties of the eigenvalues by examining the ratios between the smallest and the largest eigenvalue (c/a), and the intermediate and the largest eigenvalue (b/a), in Fig. 1. Each point corresponds to one galaxy, whose eigenvalues are associated with the cell it occupies. Unlike, for example, shape measurements (where all eigenvalues are positive and the ratios are naturally bounded), here the eigenvalues can take both positive and negative values, resulting in unbounded ratios. As a consequence, the axes in this figure are truncated at arbitrary limits, beyond which the density of points becomes negligible.

This plot visually demonstrates that the distribution of eigenvalue ratios is continuous, with no obvious natural divisions or discrete categories emerging in this plane. For reference, we have color-coded the data according to the standard discrete classification of the cosmic web into knot (red points), filament (blue points), wall (green points), and void (magenta points). For this classification, we used the threshold $\lambda_{th} = 0$. The size of the magenta points, corresponding to galaxies located in regions that are expanding along all three orthonormal axes (voids), has been arbitrarily increased for visibility, as they are very sparse. In this figure, it is important to distinguish different regions according to the values of the eigenvalues, which imply regions of compression or expansion. When the three eigenvalues are positive (0 < b/a < 1) and 0 < c/a < 1), implies regions that are collapsing on the three axes. When two of them are positive and the smallest eigenvalue is negative (0 < b/a < 1 and c/a < 0), corresponds to regions that are collapsing on two axes but expanding in the third one. When only the largest eigenvalue is positive and the other two are negative (b/a < 0) and c/a < 0), suggests regions that are expanding on two axes but collapsing in the third one. Finally, when all three eigenvalues are negative (b/a > 1 and c/a > 1), it notices regions that are expanding in the three directions, indicating the lowest dense regions of the Universe. The dotted black lines delineate the regions that the eigenvalue ratios may occupy. The horizontal dotted black line at b/a = 1 indicates that b/a < 1 whenever a > 0. The only case where b/a > 1 is when a < 0, which implies that the other two eigenvalues, b and c, are also negative, corresponding to the region known as voids. The positively sloped dotted black line indicates the condition a > b > c, which implies b/a > c/a if a > 0 (the case for knots, filaments, and walls) and b/a < c/aif a < 0 (voids). Lastly, the area inside the triangle demarcated by orange lines corresponds to $\delta > 0$, while the region outside this triangle corresponds to $\delta < 0$. In this figure, it is evident that the separation between knots, filaments, and walls depends exclusively on the chosen value of λ_{th} ; in this case, $\lambda_{th} = 0$.

4. Dependence of galaxy properties on the environment

Several studies have been conducted to comprehend the influence of the environment on galaxy formation and evolution, proving that the environment plays a fundamental role in both the formation and evolution of galaxies. There is ample evidence that the properties of galaxies and galaxy systems depend on their environment (Dressler 1980; Kauffmann et al. 2004; Blanton et al. 2005; O'Mill et al. 2008; Peng et al. 2010; Wetzel et al. 2012; Zheng et al. 2017; Wang et al. 2018; Duplancic et al. 2020, among others). For example, it is well known that stellar mass is strongly correlated with the environment. The stellar mass distribution of galaxies shifts by almost a factor of 2 toward higher masses between low- and high-density regions (Kauffmann et al. 2004). Analyzing the morphology, elliptical galaxies are more frequently located in denser regions, while spiral galaxies are more common in the field (Dressler 1980; Kuehn & Ryden 2005; Tempel et al. 2011; Pfeffer et al. 2023). Similar trends are observed for colors, star formation rate (SFR), and the ages of galaxies (Blanton et al. 2005); in denser environments, there is a higher proportion of red and passive galaxies for a given stellar mass (Baldry et al. 2006; Wetzel et al. 2012; Wang et al. 2018). Kauffmann et al. (2004) conclude that the galaxy property most sensitive to the environment is the specific star formation rate (sSFR; defined as SFR/ M_{\star}).

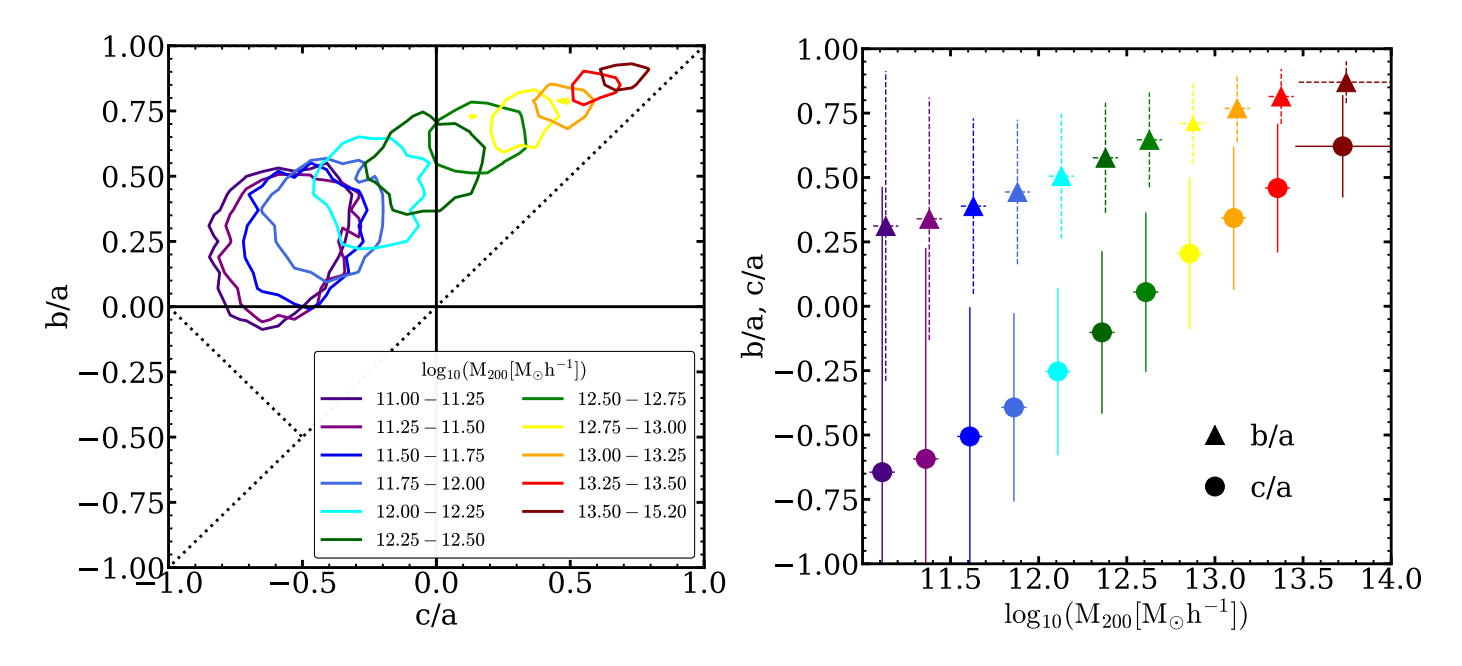


Fig. 2: Eigenvalue ratios, b/a and c/a, as a function of the logarithm of the halo mass (M_{200}) . Left panel: b/a as a function of c/a in bins of the logarithm of halo mass. This panel shows a zoomed-in view of the region displayed in Fig. 1, centered at origin. The dotted black lines delineate the regions that the eigenvalue ratios may occupy. The upper limit of the graph, b/a = 1, indicates that b/a < 1 whenever a > 0. The positively sloped dotted black line indicates the condition a > b > c, which implies b/a > c/a if a > 0 and b/a < c/a if a < 0. Right panel: Median values of b/a (triangles) and c/a (circles) for equal bins of the logarithm of the halo mass, as a function of the logarithm of the halo mass. In both panels, each color corresponds to each halo mass bin, as indicated by the legend.

They show that for galaxies with stellar masses in the range $10^{10}-3\times 10^{10}M_{\odot}$, the median sSFR decreases by more than a factor of 10 as the population shifts from predominantly star-forming at low densities to predominantly passive at high densities. This decrease is less marked but still significant for high-mass galaxies. Bamford et al. (2009) analyze the relationships between galaxy morphology, color, environment and stellar mass. They conclude that color and morphology are both sensitive to stellar mass. However, at fixed stellar mass, while color is also highly sensitive to the environment, morphology displays much weaker environmental trends. In any case, despite all the studies carried out so far, understanding the effects of the environment on galaxy properties remains a complex and active area of research.

In light of the numerous studies highlighting the role of the environment in galaxy formation and evolution, we aim to revisit these studies using a complementary approach—one that relies on a continuous, rather than discrete, characterization of the large-scale environment. In this framework, we examined how various galaxy properties correlate with their surrounding environment, as described by this continuous method. As a first step, we analyzed the values of the eigenvalue ratios b/a and c/ato identify the regions where galaxies preferentially reside, as a function of their DM halo mass. The left panel of Fig. 2 shows the relation between the ratios of eigenvalues, b/a as a function of c/a, for the galaxies sample, in bins of the logarithm of their DM halo mass (M_{200}). Each contour corresponds to each mass bin (color indicated by the legend), centered at the maximum of each sample indicating the 80 per cent. It is evident that galaxies hosted by more massive halos are located in denser regions, where both b/a and c/a increase, approaching values close to unity in regions where $\delta > 0$. Conversely, galaxies residing in less massive DM halos are found in regions where the values of b/a and c/a decrease, in some cases even reaching negative values. While there is a clear dependence of DM halos mass on the environment where galaxies inhabit, this variation is smooth. Another way to analyze this dependence is by studying the variation of the ratios of eigenvalues as a function of the DM halos mass, as shown in the right panel of Fig. 2. This figure presents the median values of b/a (triangles) and c/a (circles) in bins of the logarithm of the DM halos mass, where each color corresponds to a different DM halos mass bin, as indicated by the legend. The median value of b/a increases as we consider galaxies with more massive DM halos. As we consider environments of galaxies hosted by less massive DM halos, around $M_{200} \sim 10^{11} \,\mathrm{M_\odot} \,h^{-1}$, toward environments of galaxies hosted by more massive DM halos $(M_{200} \sim 10^{13.5} \,\mathrm{M_\odot} \,h^{-1})$, b/aincreases from $b/a \sim 0.30$ to $b/a \sim 0.85$. Despite this mass dependence, the median values of b/a remains positive within the considered mass range. On the other hand, the median values of c/a also increase as we consider galaxies with more massive DM halos. The variation in c/a values with mass is significantly greater than the variation in b/a. Median values of c/a are negative for galaxies within less massive DM halos and become positive for those within more massive halos. The median c/a is approximately $c/a \sim -0.65$ for galaxies hosted by less massive halos $(M_{200} \sim 10^{11} \,\mathrm{M}_\odot \,h^{-1})$. The transition from negative to positive c/a values occurs at $M_{200} \sim 5 \times 10^{12} \,\mathrm{M}_{\odot} \,h^{-1}$, reaching values of approximately $c/a \sim 0.60$ for galaxies hosted by more massive DM halos $(M_{200} \sim 10^{13.5} \,\mathrm{M}_{\odot} \,h^{-1})$.

In summary, both the right and left panels of Fig. 2 clearly show that the relationship between DM halos mass and the

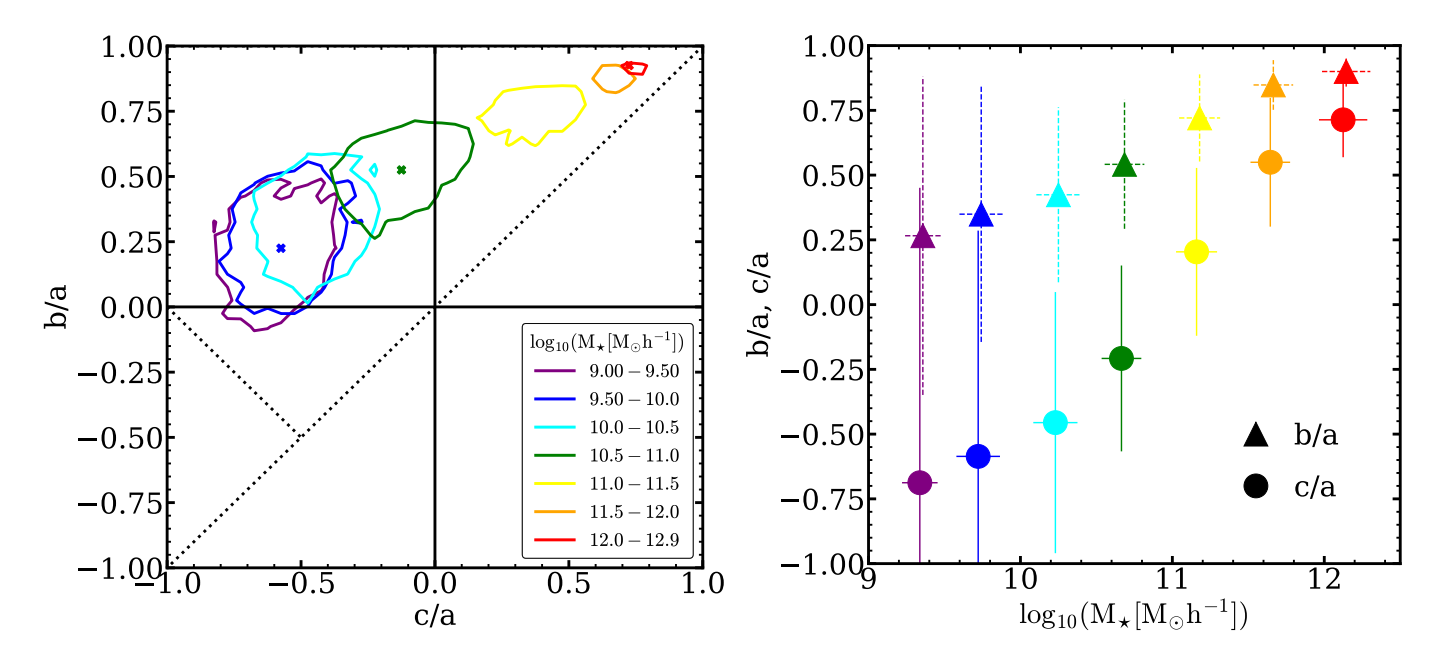


Fig. 3: Eigenvalues ratios, b/a and c/a, as a function of the logarithm of the stellar mass (M_{\star}). Left panel: Eigenvalues ratios, b/a vs. c/a, in bins of the logarithm of stellar mass. Right panel: Median values of b/a (triangles) and c/a (circles) for equal bins of the logarithm of the stellar mass, as a function of the logarithm of the stellar mass. In both panels, each color corresponds to each stellar mass bin, as indicated by the legend.

environment where galaxies are situated is continuous. We notice that the mass at which the median value of c/a transitions from negative to positive is tantalizing close to the characteristic mass discussed by Dekel & Birnboim (2006). They examine the impact of a critical halo mass in governing the bimodality of galaxy properties by modulating gas inflow, star formation, and feedback processes, ultimately driving the transition from blue star-forming disks to red passive spheroids.

Figure 3 shows the relationship between the eigenvalue ratios, b/a and c/a, similar to Fig. 2, but in this case, considering bins in the logarithm of stellar mass of galaxies (M_{\star}) . As expected, the variation of the environment according to M_{\star} is consistent with the previously presented results for the DM halos mass (M_{200}) . In the right panel of Fig. 3, more massive galaxies are located preferably in denser environments where the median values of b/a and c/a are both positive. As we consider less massive galaxies, both the values of b/a and c/adecrease, indicating that these galaxies reside in less dense environments. As we consider environments of less massive galaxies, around $M_{\star} \sim 10^9 \, \mathrm{M}_{\odot} \, h^{-1}$, toward environments of more massive galaxies $(M_{\star} \sim 10^{12} \, \mathrm{M}_{\odot} \, h^{-1})$, b/a increases from $b/a \sim 0.25$ to $b/a \sim 0.90$. Despite the variation in b/a, its median values always remain positive, indicating that the two major axes are always positive. In contrast, when analyzing the variation of c/a with respect to stellar mass, we observe that environments of less massive galaxies correspond to negative values of c/a. The median c/a is approximately $c/a \sim -0.75$ for the least massive galaxies $(M_{\star} \sim 10^9 \,\mathrm{M}_{\odot} \,h^{-1})$. These values become positive for intermediate stellar mass galaxies, around $M_{\star} \sim 10^{11} \,\mathrm{M}_{\odot} \,h^{-1}$, reaching values of approximately $c/a \sim 0.75$ for the most massive galaxies $(M_{\star} \sim 10^{12} \, \mathrm{M}_{\odot} \, h^{-1})$. As highlighted in Fig. 2, it is evident that the variation in c/a is significantly greater than the variation in b/a as a function of

stellar mass.

We display the spatial distribution of our galaxies sample in Fig. 4, in a slice of $1 \,\mathrm{Mpc}\,h^{-1}$ thickness in a box of the SMDPL simulation. The background is the same for all three panels and shows the logarithm of the density contrast estimated from DM particles, where colors are indicated by the color bar. The white filled circles represent galaxies located in environments where the values of their eigenvalue ratios b/aand c/a (corresponding to the cell in which they are located) fall within a circle of radius $0.1 \,\mathrm{Mpc}\,h^{-1}$ centered on the peaks of three of the contours in Fig. 3. Each of these centers is marked with a cross in the left panel of Fig. 3. Left panel corresponds to blue cross (c/a = -0.57, b/a = 0.22), middle panel to green cross (c/a = -0.12, b/a = 0.52) and right panel to red cross (c/a = 0.72, b/a = 0.92). From left to right, the galaxies selected are located in increasingly dense regions. Moreover, considering the trend observed in Fig. 3 and Fig. 2, as we move toward higher densities, the galaxies become more massive, which explains their lower abundance. Less massive galaxies are significantly more numerous than their massive counterparts, so the number of galaxies decreases from left to right across the three panels.

While this work presents results based solely on cosmological simulations, the proposed description of the cosmic web can also be applied to observational data. Next-generation galaxy surveys, such as the Dark Energy Spectroscopic Instrument (DESI; DESI Collaboration et al. 2016a,b) and the Vera C. Rubin Observatory's Legacy Survey of Space and Time (LSST; Ivezić et al. 2019), among others, will map an unprecedented volume of the Universe. These ambitious efforts will enable significant progress in our understanding of cosmic structure and evolution, underscoring the need for robust and efficient techniques to reconstruct the 3D DM density, velocity, and

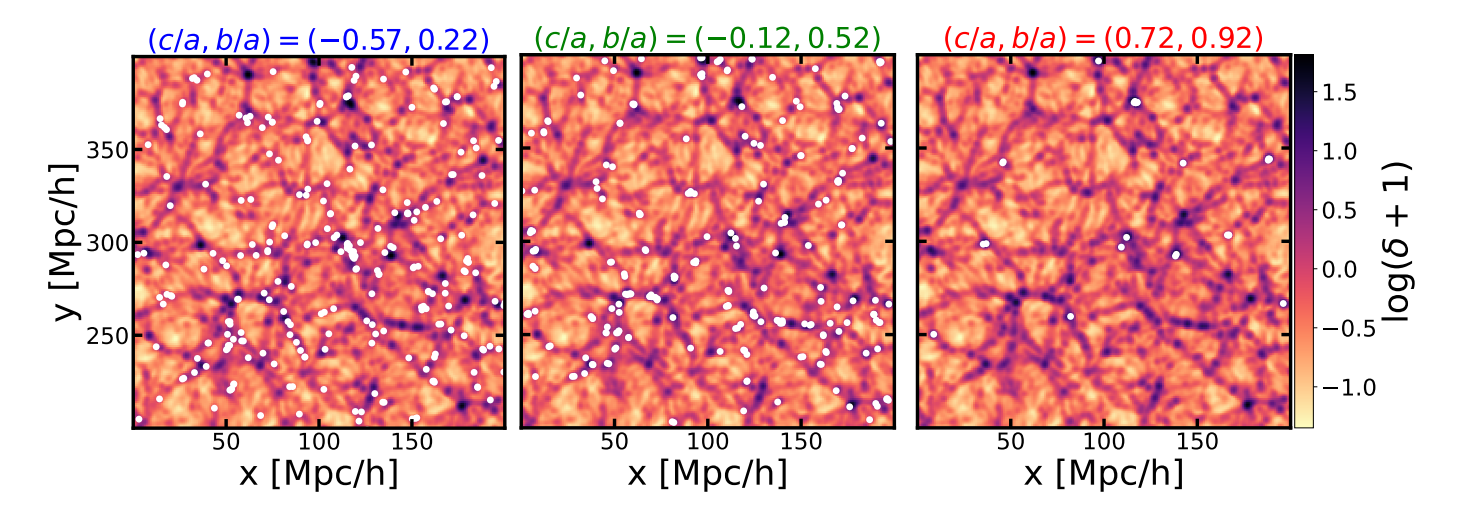


Fig. 4: Spatial distribution of central galaxies, in a slice of $1 \text{ Mpc} \, h^{-1}$ in a box of the smopl simulation. The background shows the logarithm of the density contrast estimated from DM particles, where the colors correspond to the values indicated in the color bar. White filled circles represent galaxies located in environments where the values of their eigenvalue ratios b/a and c/a (corresponding to the cell in which they are located) fall within a circle of radius $0.1 \text{ Mpc} \, h^{-1}$ centered on the peaks of three of the contours in the left panel of Fig. 3 marked with crosses. The panels correspond to the blue (left), green (middle), and red crosses (right). Above each panel, the (c/a, b/a) values are indicated for each cross.

tidal fields from extensive galaxy survey datasets. A number of studies have addressed the reconstruction of these fields from observational data (Fisher et al. 1995; Zaroubi et al. 1995; Schmoldt et al. 1999; Mathis et al. 2002; Erdoğdu et al. 2004; Wang et al. 2009; Pen et al. 2012; Wang et al. 2013, 2024; Lamman et al. 2024). Among the most recent developments, Shi et al. (2025) introduced a robust machine-learning-based framework for reconstructing the DM density, velocity, and tidal fields from DESI-like bright galaxy samples. Their approach builds upon the deep-learning method for recovering the DM density field from the redshift-space distribution of DM halos presented in Wang et al. (2024), incorporating enhancements that account for realistic observational effects, such as geometric selection, flux-limited samples, and redshift space distortions. While the model developed by Shi et al. (2025) is trained and validated using mock samples of the DESI bright galaxy survey, its design allows direct applications to real observational data. To do so, one requires a galaxy redshift survey with spectroscopic redshifts, angular positions (RA, Dec), and photometry (e.g., z-band magnitudes), along with a well-characterized survey footprint and angular mask to account for regions of incompleteness or contamination. The input to the model is the 3D galaxy overdensity field in redshift space, constructed from the observed galaxy distribution using the assumed cosmology, without requiring knowledge of peculiar velocities or DM properties. This enables the framework to infer the underlying DM density, velocity, and tidal fields directly from observable quantities. Their results demonstrate that the proposed framework accurately captures the large-scale distribution and dynamics of DM while effectively addressing key observational systematics. These advances provide a reliable and versatile tool for analyzing data from current and upcoming galaxy surveys. Once the dark tidal fields have been reconstructed from observational data using any of the currently available methods, the same procedure described earlier can be applied to estimate the eigenvalues of the tidal field and provide a continuous description of the cosmic web.

5. Galaxies properties

Galaxies properties, including stellar mass, color, and SFR, are known to exhibit strong correlations with one another, which can be influenced by environmental factors. In particular, there is a significant dependence of galaxy properties on their stellar mass. Less massive galaxies tend to be bluer and have higher SFRs compared to more massive galaxies, which are redder and exhibit lower SFRs. Moreover, the way in which galaxy properties are influenced by the environment is an ongoing area of study. As previously mentioned, one of the most commonly used methods for studying the variation of galaxy properties according to their environment is to classify the environment into discrete categories, defined based on different methods.

In this work we studied the influence of the environment on the main properties of galaxies in a continuous way, by analyzing the eigenvalues ratios estimated from the distribution of matter in the environment. Given the well-known dependence of galaxy properties on their stellar mass, in Fig. 5 we analyze how the environment in which a galaxy resides affects this dependence. Each row shows a galaxy property as a function of the stellar mass $(M_{\star}[M_{\odot}h^{-1}])$, from top to bottom: DM halo mass $(M_{200}[M_{\odot}h^{-1}])$, color (g-r), sSFR $(sSFR[yr^{-1}])$, and gas fraction $(M_{\rm gas}/(M_{\rm gas}+M_*))$. Left panels display the dependence of these properties with the environment expressed in terms of equal bins of b/a, while middle panels show them in equal bins of c/a. Each solid colored line corresponds to one of these bins, as indicated by the legends in each panel, with the number of galaxies in the bin in parentheses. As b/a and c/a increase, approaching 1, they indicate galaxies located in increasingly dense environments. However, the bins corresponding to b/a > 1 and c/a > 1, indicated with pink color, correspond to low-density regions (δ < 0). This is why these latter bins contain very few galaxies, which are distributed over a very narrow range of stellar mass, and their behavior deviates from the trend observed for the rest of the bins. The number of galaxies located in this environment is only the 0.2 per cent of the sample. In addition to the solid lines in different colors, each panel also includes a solid gray line representing median values of the entire sample analyzed. This gray line is the same across all three panels in each row. Each main panel is accompanied by a lower panel that shows the difference (Δ) between each colored line and the gray line representing the total sample. It is noteworthy that the dependence of galaxy properties on their environment, as analyzed through these ratios, is biparametric, jointly dependent on both b/a and c/a. However, when comparing the left and middle panels for each property, the most significant variations occur when considering changes in c/a. This suggests that the relationship between eigenvalue c/a is the most sensitive indicator of the dependence of galaxy properties on their environment. For comparison, the right panels show the traditional classification of environments, categorizing galaxies into four types: knots, filaments, walls, and voids. This classification is based on the criteria outlined in Section 3, with a threshold value of $\lambda_{th} = 0$. Using the eigenvalues of the environment surrounding each galaxy in our sample, we assigned each galaxy to one of these four categories.

The upper panels of Fig. 5 clearly reveal the well-known correlation between a galaxy's stellar mass (M_{\star}) and the mass of its DM halo (M_{200}): more massive galaxies tend to reside in more massive halos. Assessing the influence of the environment on this relation (as indicated by the differently colored curves) we find a dependence on the surrounding cosmic environment, particularly evident in the trends associated with the eigenvalue ratio c/a. In the left panel, where the colored curves represent different values of the intermediate-to-major eigenvalues ratio b/a, there are no significant differences among the curves, suggesting that this relation is largely insensitive to variations in b/a. In contrast, the upper-middle panel, where the colored curves correspond to different values of the minor-to-major eigenvalues ratio c/a, reveals a clear environmental dependence. Low-stellar-mass galaxies, with $\log_{10}(M_{\star}[M_{\odot}h^{-1}]) \le 10.8$, tend to inhabit less massive DM halos when located in regions where 0.5 < c/a < 1 (red line). Conversely, galaxies with $\log_{10}(M_{\star}[M_{\odot}h^{-1}]) > 10.8$ are found in more massive halos when residing in regions with 0.5 < c/a < 1 (red line). Adopting a fixed smoothing scale can affect the interpretation of environmental effects on galaxy-halo connections, potentially introducing scale-dependent features that are not of physical origin. With a fixed smoothing length, the region probed varies with the halo mass, which results in different environmental scales sampled for low and high mass halos. To assess the robustness of our findings, we repeated the analysis presented in Fig. 5 using larger smoothing scales: 2 and 4 Mpc h^{-1} , shown in Fig. A.3 and Fig. A.4, respectively, in the Appendix. As previously noted, a marked change in behavior emerges around $\log_{10}(M_{\star}[M_{\odot}h^{-1}]) \sim 10.8$ when using the original smoothing scale of 1 Mpc h^{-1} . However, this transition shifts to a higher stellar mass of $\log_{10}(M_{\star}[M_{\odot}h^{-1}]) \sim 11.2$ when adopting a smoothing scale of 2 Mpc h^{-1} and disappears entirely when the largest scale is applied. At $4 \,\mathrm{Mpc}\,h^{-1}$, galaxies across the entire stellar mass range consistently exhibit the same trend, i.e., those residing in regions where 0.5 < c/a < 1 inhabit less massive halos than galaxies of the same stellar mass located in regions with smaller c/a values. When comparing this to the right panel, which uses traditional environmental classification, the same trend is observed but is notably more attenuated. Examining the differences shown in the bottom panels (Δ) reveals that the variations are significantly more pronounced when considering c/a rather than the traditional

classification. This comparison underscores the added value of describing the environment through eigenvalue ratios, providing a complementary perspective to traditional methods: it offers a straightforward and continuous characterization that naturally reveals the dependence of galaxy properties on their surrounding environment. It is also worth noting that the lack of a significant trend with b/a is not unexpected. In regions where matter collapses nearly isotropically, b/a is inherently constrained between c/a and 1 (i.e., $c/a \le b/a \le 1$), limiting its dynamical range. While b/a might still hold some discriminatory power in differentiating between regions where matter collapses in one or two directions, our analysis reveals no strong signal across that interface, suggesting its role in tracing environmental effects is subdominant compared to c/a.

When considering color and SFR, blue galaxies are typically lower-mass systems that are actively forming stars, whereas red galaxies tend to be more massive and have largely ceased star formation. The transition from blue to red galaxies occurs through a process known as quenching, where star formation declines resulting in a redder color. The second row panels show the dependence of color (g-r), where it is evident that more massive galaxies are redder, while less massive ones are bluer. Taking the environment into account, particularly focusing on c/a, there is a clear trend for galaxies of comparable stellar mass: for a given stellar mass, galaxies tend to become progressively redder as the values of c/a increase toward unity, which corresponds to regions with $\delta > 0$. This trend is noticeable for galaxies with $\log_{10}(M_{\star}[M_{\odot}h^{-1}]) < 10.8$, but becomes negligible for more massive galaxies. Concerning the sSFR shown in the third-row panels, it displays a pattern similar to that of color and admits a similar analysis: galaxies located in regions where the c/a value is close to 1 (with $\delta > 0$), tend to have lower SFRs, suggesting they are more quiescent compared to galaxies of similar stellar mass found in regions with lower c/a values. This trend is again observed for galaxies with $\log_{10}(M_{\star}[M_{\odot}h^{-1}]) < 10.8$. Finally, we analyzed the gas fraction of galaxies and its dependence on the environment (bottom panels). The relationship between gas fraction and stellar mass is closely linked to SFR and galaxy color. It is well established that lower-mass galaxies have a higher gas fraction available for star formation, which also contributes to their bluer color. In contrast, more massive galaxies have less gas available for star formation, making them redder and more quiescent. When examining the environmental dependence, a trend similar to that observed for galaxy color and sSFR emerges: lower-mass galaxies exhibit a reduced gas fraction in regions where the c/a values increase and approach unity, which corresponds to regions with $\delta > 0$. However, unlike the trend seen for color and sSFR, where more massive galaxies show no significant environmental variation, in the case of gas fraction, more massive galaxies reverse this pattern, displaying a higher gas fraction when c/a value becomes closer to 1 ($\delta > 0$). As previously discussed when analyzing the variation in the dependence of halo mass on stellar mass according to the environment in which galaxies reside, the observed change in the trend at the high-mass end is not a physical effect but rather a consequence of using a smoothing scale that is small relative to the size of the most massive galaxies. When the smoothing scale is increased, this trend disappears. Using a smoothing scale of $4 \,\mathrm{Mpc}\,h^{-1}$ galaxies located in regions where c/a approaches 1 ($\delta > 0$) exhibit lower gas fractions than galaxies with the same stellar mass located in regions with smaller c/a values. This trend is consistent across the entire range of stellar masses analyzed

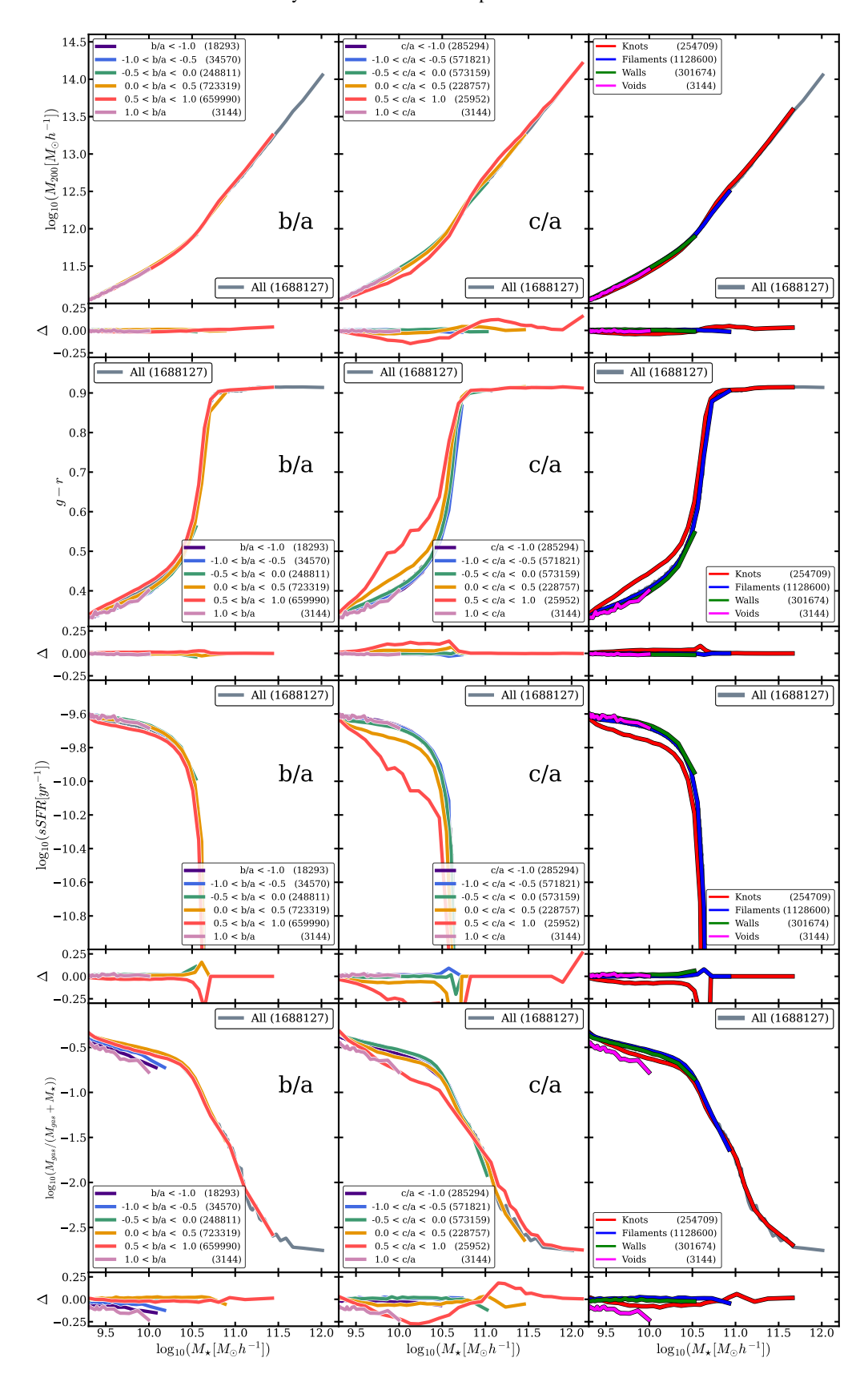


Fig. 5: Galaxy properties as a function of the logarithm of the stellar mass. From top to bottom: Logarithm of DM halo mass, color (g-r), logarithm of the sSFR, and logarithm of the gas fraction. Each column displays the dependence of these properties on the environment: equal bins in b/a (left panels) and equal bins in c/a (middle panels). Each solid colored line corresponds to one of these bins, as indicated by the legends in each panel. Next to each bin, the number of galaxies contained within that bin is specified. The solid gray line in each panel represents the total sample. For comparison, the right panels show the dependence of these properties on the environment according to the traditional method, categorizing the environment into four types: knots, filaments, walls, and voids. Each main panel is accompanied by a lower panel that shows the difference (Δ) between each colored line and the gray line.

Article number, page 9 of 18

(please, see Fig. A.4 in the Appendix). This trend is also evident in the right panel, although it is much less pronounced.

In summary, the continuous description of the cosmic web offers a complementary and detailed perspective on the environmental dependence of galaxy properties. Its continuous nature allows for the identification of subtle trends and smooth variations. Notably, the mean trends observed using c/a align with those obtained through the traditional classification, indicating that our method is consistent with previous findings while offering enhanced detail.

For completeness, we present Fig. 6, which is similar to Fig. 5 but shows galaxy properties as a function of DM halo mass (M_{200}) instead of stellar mass. Comparing these figures, it is evident that they display very similar trends. As in Fig. 5, all properties show a more pronounced dependence on the environment when considering the eigenvalue ratio c/a. Comparing galaxies residing in DM halos of similar mass, those located in environments with c/a close to 1 (δ > 0) are redder, exhibit lower SFRs, and have a lower gas fraction. This environmental dependence is significant only for galaxies whose DM halos are less massive than $M_{200} = 10^{12}$.

6. Conclusions

In this work we present a new continuous description of the cosmic web using the ratios of the eigenvalues of the Hessian matrix derived from the matter distribution. We applied this method to a numerical simulation coupled with a semi-analytic model of galaxy formation and analyzed the dependence of galaxy properties on the environment.

Galaxy properties show a clear dependence on the surrounding environment. More massive galaxies, which tend to be redder, quenched, and gas-poor, are most commonly found in regions where the eigenvalues a, b, and c are roughly equal. In contrast, lower-mass galaxies, typically bluer, star-forming, and gas-rich, are more likely to reside in environments where the values of b/a and c/a decrease. While the properties of the most massive galaxies show little sensitivity to environmental factors, low-mass galaxies are significantly more influenced by their surroundings. Although the environmental dependence of galaxy properties is biparametric, as it is jointly dependent on both b/a and c/a, it is predominantly driven by the eigenvalue ratio c/a.

We compared our results with those obtained using the traditional method of classifying environments into four categories: knots, filaments, walls, and voids. Our new eigenvalue ratio method offers two key advantages. First, it eliminates the need for arbitrary thresholds to define each environmental category. Second, the dependence of galaxy properties on the environment is much more pronounced when directly considering the eigenvalue ratio, compared to the four traditional categories. This is because the dependence becomes particularly strong in environments where the values of c/a approach unity in regions with $\delta > 0$. In this regime, the three principal axes of the matter distribution are nearly equal, indicating a more symmetric and isotropic collapse. However, when all such environments are indiscriminately grouped into a single category (knots), the subtle differences associated with varying degrees of collapse

symmetry are effectively averaged out, which dilutes the underlying trend.

Furthermore, using eigenvalue ratios enables the study of the temporal evolution of galaxy environments without introducing arbitrary thresholds that may vary over time, allowing for more direct and accurate comparisons across different epochs. These findings extend beyond the scope of this paper and will be presented in a forthcoming study.

Acknowledgements. We would like to thank the referee for carefully reading the manuscript and providing many comments and suggestions that significantly improved our paper. The SMDPL simulation was performed at LRZ Munich within the pr87yi project. The authors gratefully acknowledge funding for this project from the Gauss Centre for Supercomputing e.V. (www.gauss-centre.eu) by providing computing time on the GCS Supercomputer SUPERMUC-NG at the Leibniz Supercomputing Centre (www.lrz.de). The CosmoSim database (www.cosmosim.org) used in this paper is a service of the Leibniz Institute for Astrophysics Potsdam (AIP). This work has been partially supported by the Consejo de Investigaciones Científicas y Técnicas de la República Argentina (CONICET), Secretaría de Ciencia y Técnica de la Universidad Nacional de Córdoba (SeCyT) and Agencia Nacional de Promoción Científica y Tecnológica (PICT 2019-1600), Argentina. GY would like to thank Ministerio de Ciencia e Innovación (Spain) for financial support under the project grant PID2021-122603NB-C21. MGA and GY also thanks European Union Horizon 2020 Research and Innovation Programme for partial financial support under the Marie Sklodowska-Curie grant agreement No 734374-LACEGAL. MGA acknowledges the hospitality of the Departamento de Física Teórica at the Universidad Autónoma de Madrid during a scientific visit when part of this project was carried out.

References

Alpaslan, M., Robotham, A. S. G., Driver, S., et al. 2014, MNRAS, 438, 177 Aragón-Calvo, M. A., Platen, E., van de Weygaert, R., & Szalay, A. S. 2010, ApJ, 723, 364

Aragón-Calvo, M. A., van de Weygaert, R., Jones, B. J. T., & van der Hulst, J. M. 2007, ApJ, 655, L5

Aragon-Calvo, M. A. & Yang, L. F. 2014, MNRAS, 440, L46

Ayçoberry, E., Barthelemy, A., & Codis, S. 2024, A&A, 686, A276 Balaguera-Antolínez, A., Montero-Dorta, A. D., & Favole, G. 2024, A&A, 685, A61

Baldry, I. K., Balogh, M. L., Bower, R. G., et al. 2006, MNRAS, 373, 469 Bamford, S. P., Nichol, R. C., Baldry, I. K., et al. 2009, MNRAS, 393, 1324

Behroozi, P. S., Wechsler, R. H., & Wu, H.-Y. 2013a, ApJ, 762, 109 Behroozi, P. S., Wechsler, R. H., Wu, H.-Y., et al. 2013b, ApJ, 763, 18

Blanton, M. R., Eisenstein, D., Hogg, D. W., Schlegel, D. J., & Brinkmann, J. 2005, ApJ, 629, 143

Bond, J. R., Kofman, L., & Pogosyan, D. 1996, Nature, 380, 603 Cautun, M., van de Weygaert, R., Jones, B. J. T., & Frenk, C. S. 2014, MNRAS,

441, 2923 Codis, S., Pichon, C., Devriendt, J., et al. 2012, MNRAS, 427, 3320

Codis, S., Pichon, C., & Pogosyan, D. 2015, MNRAS, 452, 3369
Colless, M., Peterson, B. A., Jackson, C., et al. 2003, arXiv e-prints, arXiv:0306581

Cora, S. A., Vega-Martínez, C. A., Hough, T., et al. 2018, MNRAS, 479, 2 de Lapparent, V., Geller, M. J., & Huchra, J. P. 1986, ApJ, 302, L1 Dekel, A. & Birnboim, Y. 2006, MNRAS, 368, 2

DESI Collaboration, Aghamousa, A., Aguilar, J., et al. 2016a, arXiv e-prints, arXiv:1611.00036

DESI Collaboration, Aghamousa, A., Aguilar, J., et al. 2016b, arXiv e-prints, arXiv:1611.00037

Dressler, A. 1980, ApJS, 42, 565

Duplancic, F., Dávila-Kurbán, F., Coldwell, G. V., Alonso, S., & Galdeano, D. 2020, MNRAS, 493, 1818

Erdoğdu, P., Lahav, O., Zaroubi, S., et al. 2004, MNRAS, 352, 939

Falck, B. L., Neyrinck, M. C., & Szalay, A. S. 2012, ApJ, 754, 126

Fisher, K. B., Lahav, O., Hoffman, Y., Lynden-Bell, D., & Zaroubi, S. 1995, MNRAS, 272, 885

Forero-Romero, J. E., Hoffman, Y., Gottlöber, S., Klypin, A., & Yepes, G. 2009, MNRAS, 396, 1815

Forero-Romero, J. E., Palomino, A., Gómez-Cortés, F. L., & Li, X.-D. 2025, RAS Techniques and Instruments, 4, rzaf032

Hahn, O., Carollo, C. M., Porciani, C., & Dekel, A. 2007a, MNRAS, 381, 41

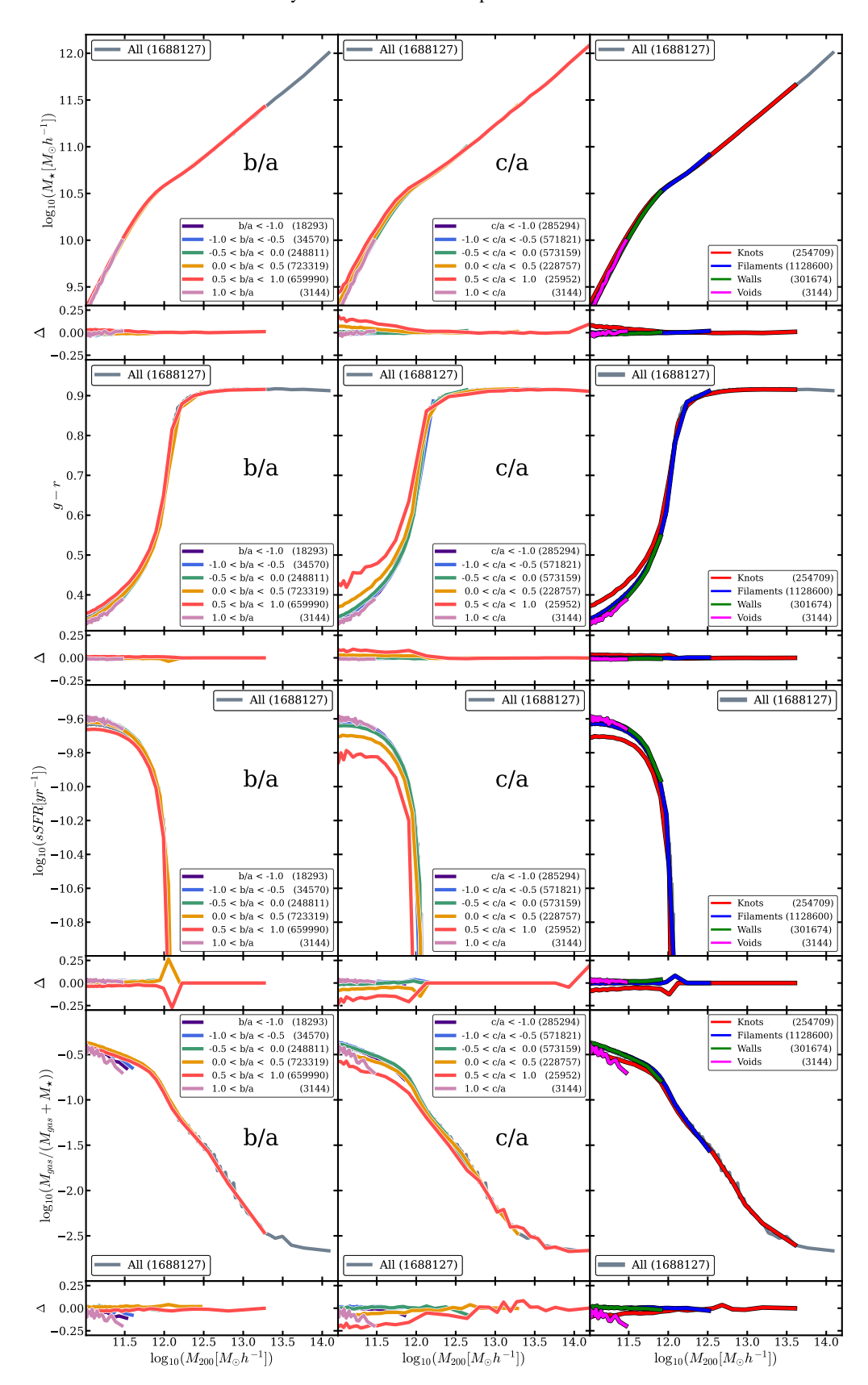


Fig. 6: Similar to Fig. 5 but as a function of the logarithm of the DM halo mass instead of the stellar mass of the galaxies.

Hahn, O., Porciani, C., Carollo, C. M., & Dekel, A. 2007b, MNRAS, 375, 489 Hahn, O., Teyssier, R., & Carollo, C. M. 2010, MNRAS, 405, 274 Hoffman, Y., Metuki, O., Yepes, G., et al. 2012, MNRAS, 425, 2049 Icke, V. & van de Weygaert, R. 1991, QJRAS, 32, 85 Ivezić, Ž., Kahn, S. M., Tyson, J. A., et al. 2019, ApJ, 873, 111
Jaber, M., Peper, M., Hellwing, W. A., Aragón-Calvo, M. A., & Valenzuela, O. 2024, MNRAS, 527, 4087

Kauffmann, G., White, S. D. M., Heckman, T. M., et al. 2004, MNRAS, 353,

713

Kennedy, J. & Eberhart, R. 1995, in Proceedings of ICNN'95-international conference on neural networks, Vol. 4, ieee, 1942–1948

Klypin, A., Yepes, G., Gottlöber, S., Prada, F., & Heß, S. 2016, MNRAS, 457, 4340

Knebe, A., Pearce, F. R., Gonzalez-Perez, V., et al. 2018, MNRAS, 475, 2936 Kuehn, F. & Ryden, B. S. 2005, ApJ, 634, 1032

Lamman, C., Eisenstein, D., Forero-Romero, J. E., et al. 2024, MNRAS, 534, 3540

Libeskind, N. I., Hoffman, Y., Forero-Romero, J., et al. 2013, MNRAS, 428, 2489

Libeskind, N. I., Hoffman, Y., Knebe, A., et al. 2012, MNRAS, 421, L137

Libeskind, N. I., Knebe, A., Hoffman, Y., & Gottlöber, S. 2014, MNRAS, 443, 1274

Libeskind, N. I., van de Weygaert, R., Cautun, M., et al. 2018, MNRAS, 473, 1195

Mathis, H., Lemson, G., Springel, V., et al. 2002, MNRAS, 333, 739

Olex, E., Hellwing, W. A., & Knebe, A. 2025, A&A, 696, A142

O'Mill, A. L., Padilla, N., & García Lambas, D. 2008, MNRAS, 389, 1763

Pen, U.-L., Sheth, R., Harnois-Deraps, J., Chen, X., & Li, Z. 2012, arXiv e-prints, arXiv:1202.5804

Peng, Y.-j., Lilly, S. J., Kovač, K., et al. 2010, ApJ, 721, 193

Pfeffer, J., Cavanagh, M. K., Bekki, K., et al. 2023, MNRAS, 518, 5260

Pfeifer, S., Libeskind, N. I., Hoffman, Y., et al. 2022, MNRAS, 514, 470

Planck Collaboration, Ade, P. A. R., Aghanim, N., et al. 2014, A&A, 571, A16

Ruiz, A. N., Cora, S. A., Padilla, N. D., et al. 2015, ApJ, 801, 139

Schmoldt, I. M., Saar, V., Saha, P., et al. 1999, AJ, 118, 1146

Shandarin, S. F. 2004, MNRAS, 353, 163

Shandarin, S. F., Habib, S., & Heitmann, K. 2012, Phys. Rev. D, 85, 083005

Shandarin, S. F. & Zeldovich, Y. B. 1989, 61, 185

Shi, F., Wang, Z., Yang, X., et al. 2025, ApJS, 280, 53

Sousbie, T. 2011, MNRAS, 414, 350

Sousbie, T., Pichon, C., Colombi, S., Novikov, D., & Pogosyan, D. 2008, MN-RAS, 383, 1655

Springel, V., White, S. D. M., Tormen, G., & Kauffmann, G. 2001, MNRAS, 328, 726

Tegmark, M., Strauss, M. A., Blanton, M. R., et al. 2004, Phys. Rev. D, 69, 103501

Tempel, E., Saar, E., Liivamägi, L. J., et al. 2011, A&A, 529, A53

Tempel, E. & Tamm, A. 2015, A&A, 576, L5

Wang, H., Mo, H. J., Chen, S., et al. 2018, ApJ, 852, 31

Wang, H., Mo, H. J., Jing, Y. P., et al. 2009, MNRAS, 394, 398

Wang, H., Mo, H. J., Yang, X., & van den Bosch, F. C. 2013, ApJ, 772, 63

Wang, P. & Kang, X. 2017, MNRAS, 473, 1562

Wang, P., Kang, X., Libeskind, N. I., et al. 2020, New A, 80, 101405

Wang, Z., Shi, F., Yang, X., et al. 2024, Science China Physics, Mechanics, and Astronomy, 67, 219513

Wetzel, A. R., Tinker, J. L., & Conroy, C. 2012, MNRAS, 424, 232

Yaryura, C. Y., Abadi, M. G., Gottlöber, S., et al. 2023, MNRAS, 525, 415

Zaroubi, S., Hoffman, Y., Fisher, K. B., & Lahav, O. 1995, ApJ, 449, 446

Zhang, Y., Guo, H., Yang, X., & Wang, P. 2024, MNRAS, 533, 1048

Zhang, Y., Yang, X., Faltenbacher, A., et al. 2009, ApJ, 706, 747

Zhang, Y., Yang, X., Wang, H., et al. 2015, ApJ, 798, 17 Zheng, Z., Wang, H., Ge, J., et al. 2017, MNRAS, 465, 4572

Appendix A: Analyzing different smoothing scales

The influence of the smoothing scale used to categorize the cosmic web has been extensively analyzed in numerous studies (e.g., Ayçoberry et al. 2024; Zhang et al. 2024; Balaguera-Antolínez et al. 2024; Pfeifer et al. 2022; Wang et al. 2020, among others). These works demonstrate that the outcomes of different analyses are significantly affected not only by the chosen smoothing scale but also by the choice of threshold used to classify the cosmic web, depending on how many eigenvalues exceed that value. The extent of these dependences varies depending on the specific properties or phenomena under investigation. In this appendix, we demonstrate that our results remain robust under variations in the smoothing scale $(1, 2, \text{ and 4 Mpc}\,h^{-1})$ and when the shear velocity field is used instead of the tidal field to estimate the eigenvalues a, b and c.

Figure A.1 illustrates the variation in the median values of the ratio of eigenvalues b/a (left panel) and c/a (right panel) as a function of the stellar mass (solid black lines) and the halo mass (dashed black lines) for the three smoothing scales analyzed (1, 2, and 4 Mpc h^{-1}) differentiated by the thickness of the lines, as indicated in the legend. In these figures, as in all figures presented throughout the paper, the eigenvalues a, b and c were computed from the tidal field, derived from the density field of DM particles. For comparison, Fig. A.2 is equivalent to Fig. A.1, but in this case, the eigenvalues a, b and c were estimated from the shear velocity field.

From these figures, we conclude that although increasing the smoothing scale does have an impact, particularly in the higher mass bins, the overall trends persist, and our main conclusions remain robust. In our proposed method for describing the cosmic web, the c/a ratio emerges as the most effective parameter for capturing the relationship between galaxy properties and their surrounding environment. This dependence is remarkably clear and continuous across the parameter space, enabling a detailed and nuanced exploration of how galaxy properties vary with their environment.

The choice of smoothing scale used to define the cosmic web constitutes a well-known limitation affecting many of the currently employed methods, including the traditional approach that classifies the cosmic web into four distinct components (Hahn et al. 2007b; Sousbie et al. 2008; Forero-Romero et al. 2009; Libeskind et al. 2013, 2018; Wang et al. 2020; Jaber et al. 2024; Zhang et al. 2024, among others). Recognizing the relevance of the smoothing scale in characterizing the environment in which galaxies reside—and the potential impact this choice may have on the results presented in this work-we repeated our analysis of the dependence of galaxy properties on their surrounding environment, adopting different smoothing lengths for the environmental description. Figs. A.3 and A.4 present galaxy properties as a function of stellar mass, in the same manner as Fig. 5. While Fig. 5 corresponds to a smoothing length of 1 Mpc h^{-1} , Figs. A.3 and A.4 display the results obtained with smoothing lengths of 2 and 4 Mpc h^{-1} , respectively. A comparative analysis of the corresponding panels across the three figures—each based on a different smoothing scale—reveals that the most significant trends are preserved regardless of the chosen scale. The most notable difference arises in the dependence of galaxy properties on the c/a parameter. As discussed in Section 5, galaxies exhibit a stronger correlation with c/a than with b/a. Focusing on the variation of halo mass (M_{200}) with

c/a (middle upper panels), we find that when the environment is defined using a smoothing scale of 1 Mpc h^{-1} , low-stellar-mass galaxies—up to $\log_{10}(M_{\star}[M_{\odot}h^{-1}]) \sim 10.8$ —tend to reside in less massive DM halos when the values of c/a rise and tend toward unity (red line). Conversely, for galaxies with $\log_{10}(M_{\star}[M_{\odot}h^{-1}]) > 10.8$, the trend reverses: they are found in more massive halos when located in environments where the values of c/a increase, approaching unity (red line). As the smoothing scale increases, the stellar mass at which this reversal occurs also shifts to higher values. Specifically, this transition occurs at $\log_{10}(M_{\star}[M_{\odot}h^{-1}]) \sim 11.2$ when using a smoothing scale of 2 Mpc h^{-1} , and at even higher stellar masses for the 4 Mpc h^{-1} scale. For the other galaxy properties analyzed, no significant differences are observed with varying smoothing scales.

For completeness, we also include Figs A.5 and A.6, which are analogous to Fig. 6 (where astrophysical properties are analyzed as a function of the DM halo mass) but instead define the galaxy environment using smoothing scales of 2 and 4 Mpc h^{-1} , respectively. In this case as well, we find no significant differences in the results when changing the smoothing length used to define the environment of galaxies. In conclusion, as anticipated in Section 3, the main results presented in this study remain robust across different choices of smoothing length in the definition of the environment.

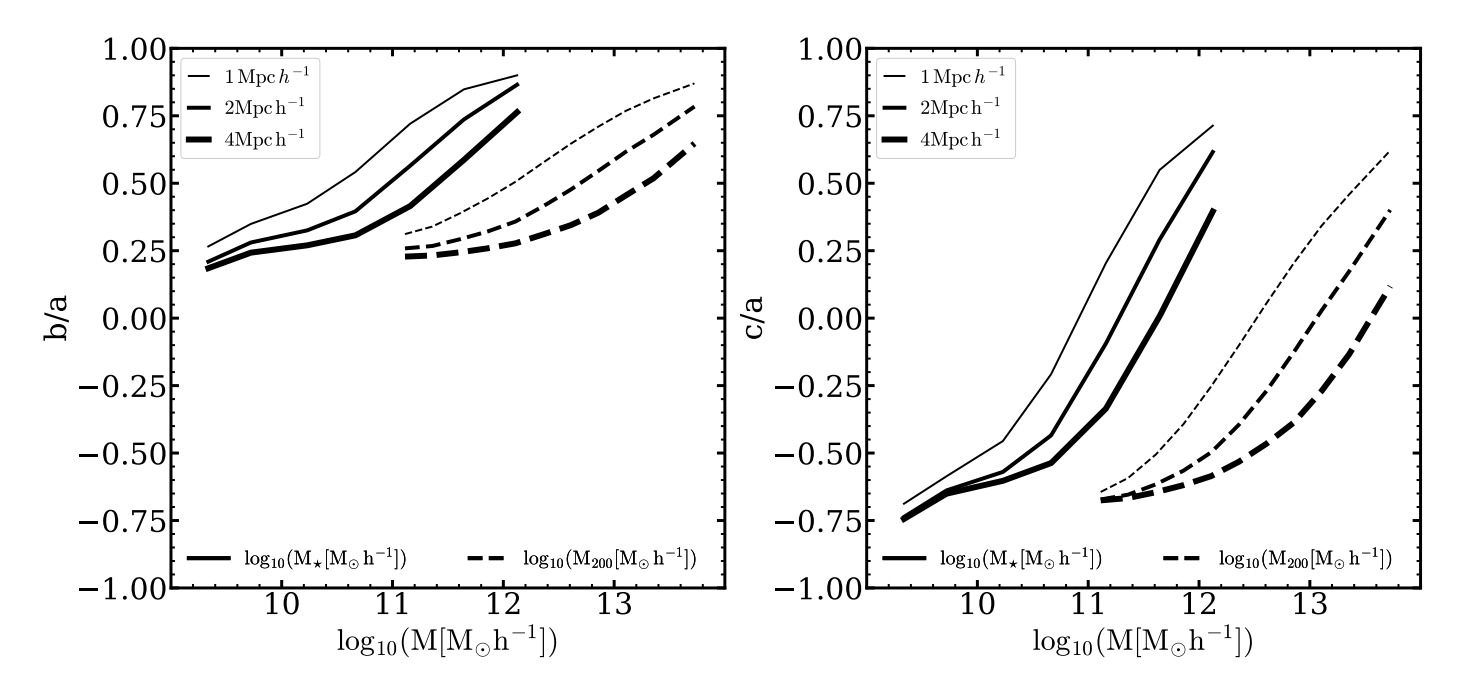


Fig. A.1: Eigenvalues ratios b/a (left panel) and c/a (right panel) as a function of the logarithm of stellar mass (solid black lines) and the logarithm of DM halo mass (dashed black lines) for the three smoothing scales analyzed (1, 2, and 4 Mpc h^{-1}) differentiated by the thickness of the lines, as indicated in the legend. Eigenvalues are estimated from the tidal tensor.

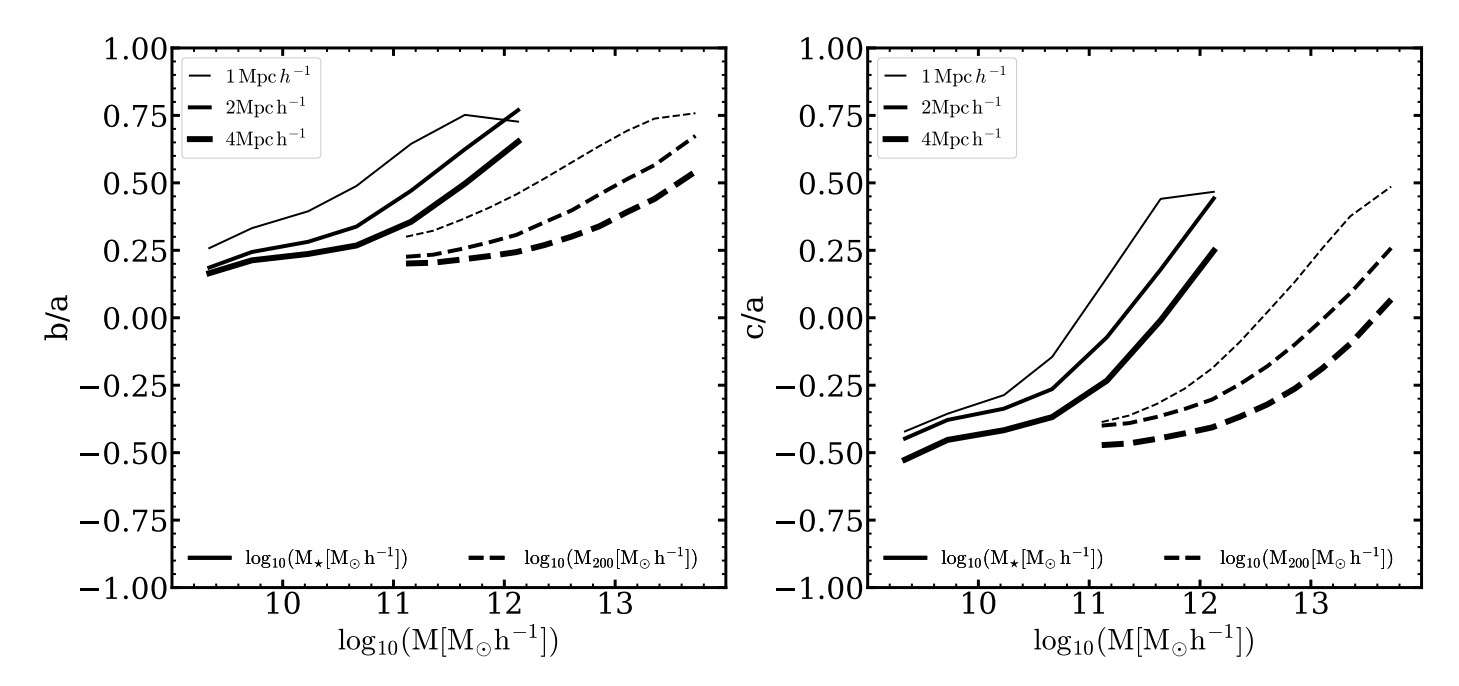


Fig. A.2: Eigenvalues ratios b/a (left panel) and c/a (right panel) as a function of the logarithm of stellar mass (solid black lines) and the logarithm of DM halo mass (dashed black lines) for the three smoothing scales analyzed (1, 2, and 4 Mpc h^{-1}) differentiated by the thickness of the lines, as indicated in the legend. Eigenvalues are estimated from the shear velocity field.

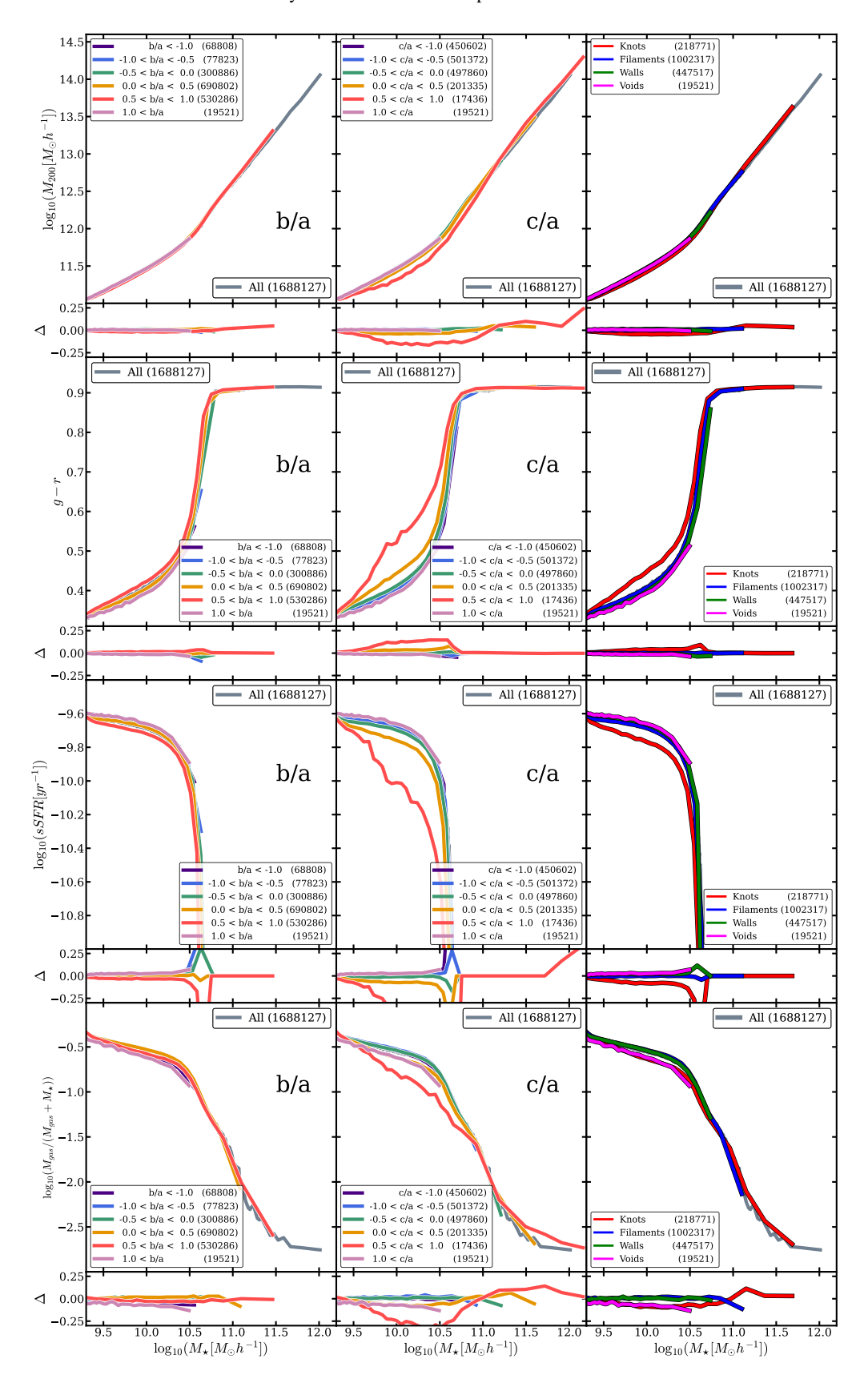


Fig. A.3: Similar to Fig. 5 but using a smoothing scale equals to 2 Mpc h^{-1} .

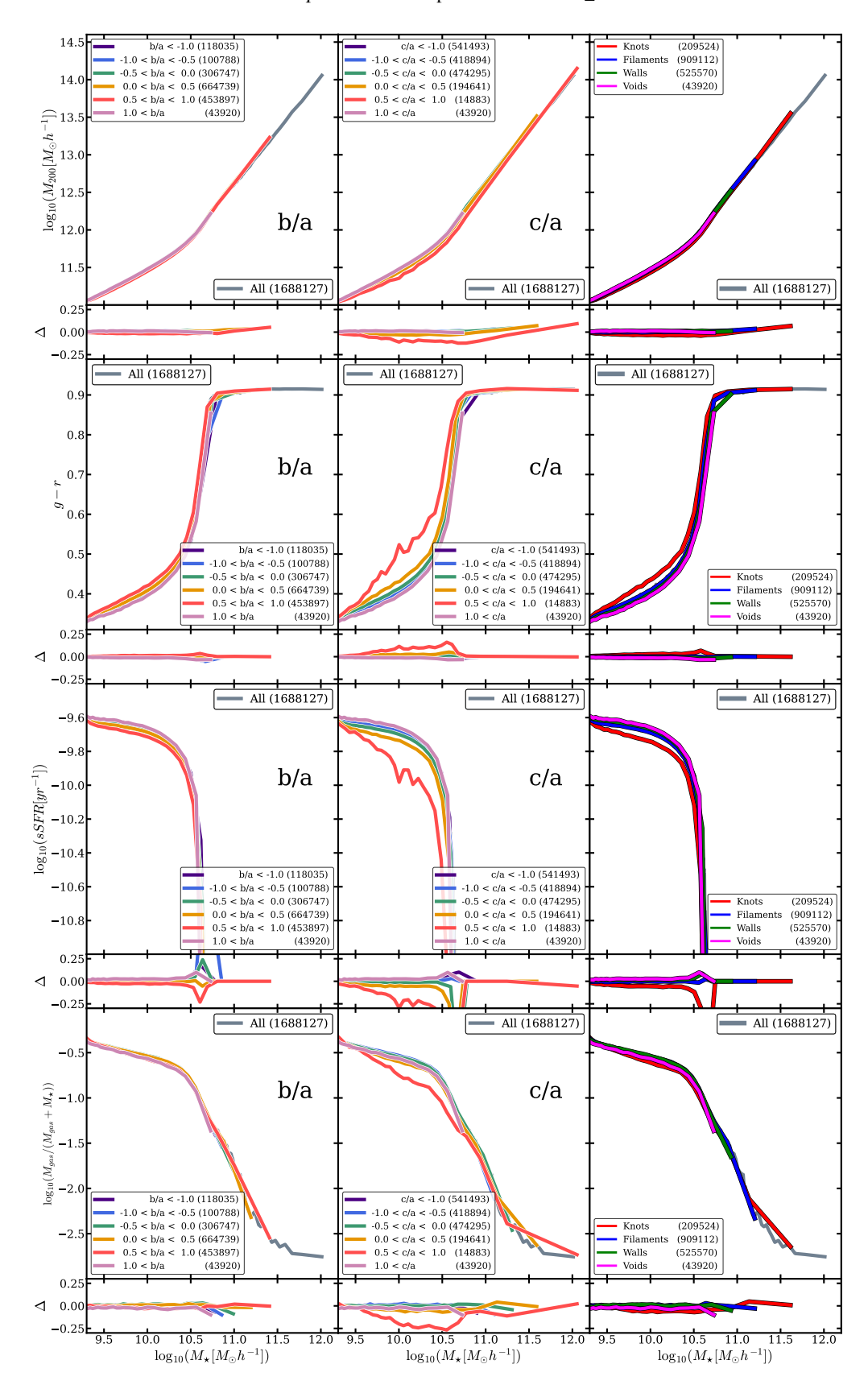


Fig. A.4: Similar to Fig. 5 but using a smoothing scale equals to 4 Mpc h^{-1} .

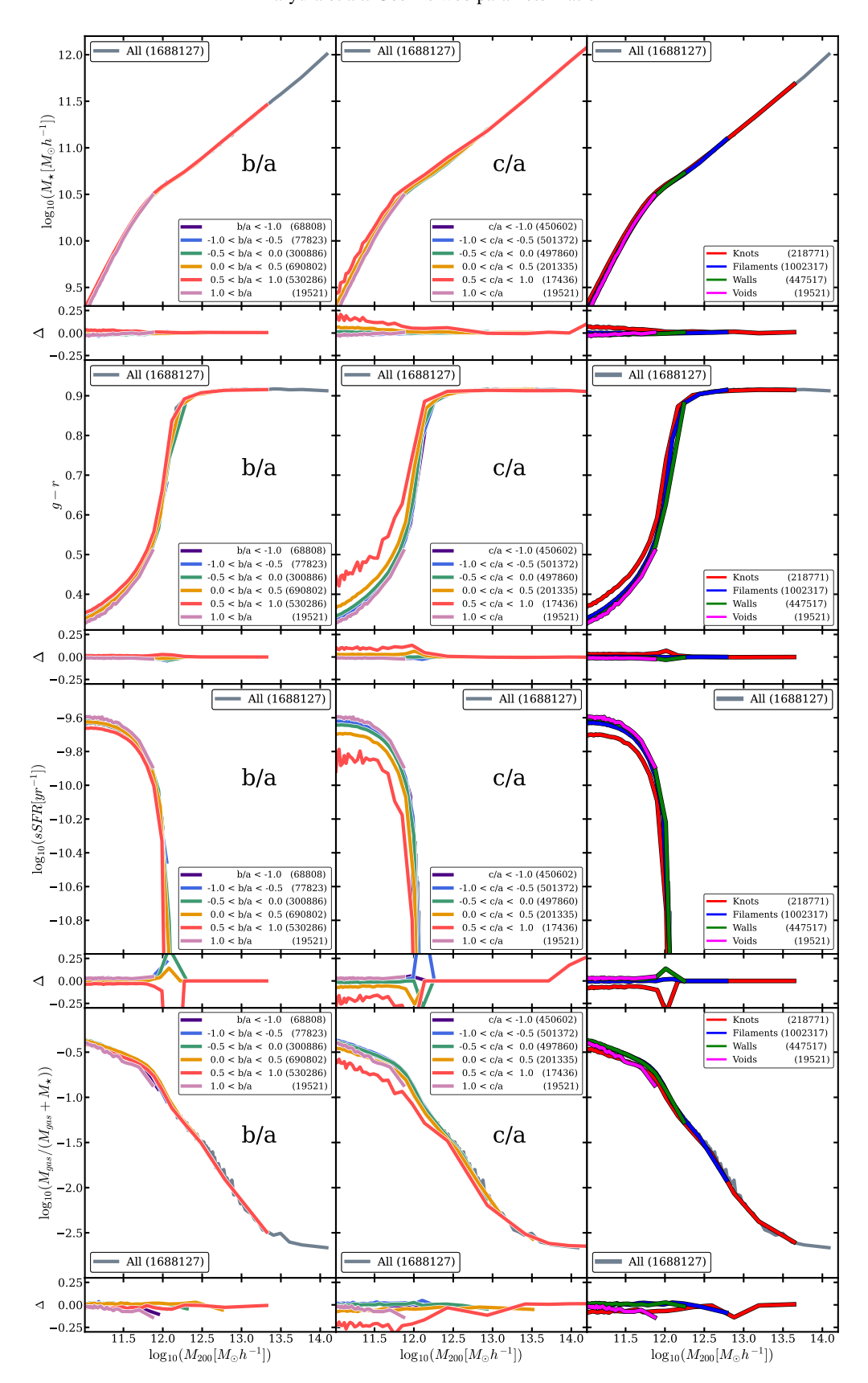


Fig. A.5: Similar to Fig. 6 but using a smoothing scale equals to 2 Mpc h^{-1} .

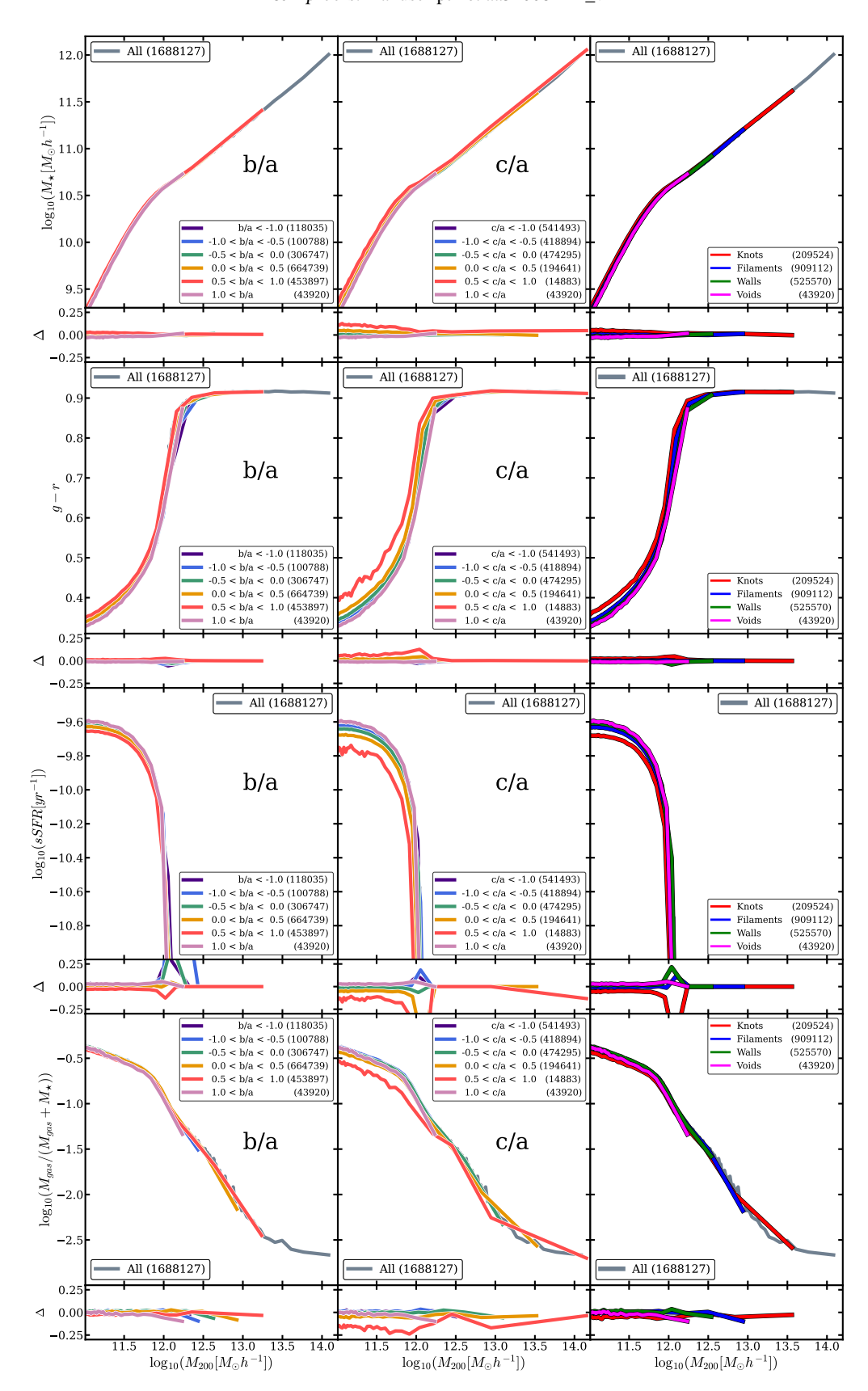


Fig. A.6: Similar to Fig. 6 but using a smoothing scale equals to 4 Mpc h^{-1} .